Interferometric redatuming using direct wavefield modeling

Tiago A. Coimbra, Diego F. Barrera*, Jörg Schleicher and Amélia Novais (University of Campinas & INCT-GP)

This paper was prepared for presentation at the 13th International Congress of the Brazilian Geophysical Society, held in Rio de Janeiro, Brazil, August 26-29, 2013.

Abstract

In recent years there has been a growing interest to improve the petroleum exploration and processing of seismic data using interferometric techniques. Seismic interferometry allows the use of parts of the information contained in the seismic data that are not taken into account in conventional processing. Its basic principle allows us to generate new seismic responses or virtual sources where only receivers were placed. In this work, we have developed an interferometric redatuming technique that uses the correlation of direct waves in a reference model with scattered waves in the true model to reposition sources and/or receivers for the latter. The correlation with the direct wave only has the advantage that this wave is generally easily accessible. If ocean-bottom or borehole receivers are available, the direct wave can be measured, or if a reference velocity model down to a desirable datum is known, it can be determined by modeling. The resulting redatuming technique has worked satisfactorily on synthetic seismic data from a three-layer model.

Introduction

Seismic interferometry is a technique based on optical physics. It allows the use of parts of the information contained in the seismic data that are not taken into account in conventional processing. Its basic principle allows us to generate new seismic responses or virtual sources where only receivers were placed (Wapenaar et al., 2010). In seismic exploration authors like Claerbout (1968) and Scherbaum (1978) were the first to make use of interferometric techniques. Claerbout (1968) showed that the Green's function for reflections recorded at the Earth's surface could be obtained by the autocorrelation of the data generated by buried sources in a 1D medium, while Scherbaum (1978), using information of microquakes, constructed geological structure based on the properties of the Green's functions.

Interferometric redatuming techniques have been studied, e.g., by Xiao and Schuster (2006), Schuster and Zhou (2006), Dong et al. (2007), Lu et al. (2008), van der Neut et al. (2011) and many others. They attempt to use the techniques with the objective of improving the seismic sections and reducing the uncertainty in hydrocarbon exploration in regions of high structural and sedimentological complexity. The redatuming technique's principal applications are the correction of seismic data for effects of an acquisition at an irregular surface and for the effects of complex geological structures in the overburden and low velocity layer. The objective is to focus the seismic data processing in a specific subsurface region.

Interferometric redatuming can be used to relocate sources to positions where only receivers are available and allows to carry the seismic acquisitions from the surface to geologic horizons of interest. In this work, we correlate the modeled direct wavefield with seismic surface data to relocate the acquisition system to any datum in the subsurface to where direct waves can be modeled with sufficient accuracy.

The derivation starts from a convenient approximation of the seismic interferometry equation using Green's theorem on the Helmholtz equation with density variation. It proceeds to the general redatuming equation and the specific approximation discussing the correlation of acquired seismic data with modeled direct waves. In the numerical results section, we apply the new redatuming method to a simple synthetic example to simulated data as if aquired with sources and receivers at the ocean bottom.

Theory

In this section we describe the basic theory of interferometry for acoustic media with density variation. We deduce the reciprocity theorem, interferometry principle and the Green's function approximation. We start at the inhomogeneous Helmholtz equation, which is written as follows

$$\rho(x)\nabla\cdot\left[\frac{1}{\rho(x)}\nabla\hat{\psi}(x,\omega)\right]+\frac{\omega^2}{v^2(x)}\hat{\psi}(x,\omega)=-\hat{F}(x,\omega), \quad (1)$$

where $\rho(x)$ is the variable density, $\hat{\psi}(x,\omega)$ is the field pressure, ω is the angular frequency, $v(x)$ is wave velocity, and $F(x,\omega)$ is the source term.

In the special case of a temporal and spatial point source, i.e., when the source term $F(x,\omega)$ is given by a delta function $\delta(x-x_A)$, the pressure field is represented by the Green's function $\hat{G}(x,\omega;x_A)$, so that the Helmholtz equation reads

$$\rho(x)\nabla\cdot\left[\frac{1}{\rho(x)}\nabla\hat{G}(x,\omega;x_A)\right]+\frac{\omega^2}{v^2(x)}\hat{G}(x,\omega;x_A)=-\delta(x-x_A). \quad (2)$$

Gauss's theorem relates an integral over a closed surface ∂E of an arbitrary vector field to an integral over the enclosed volume E of the divergence of the vector field. Choosing the vector field appropriately, this theorem can be written as (Green, 1828)

$$\oiint_{\partial E}(\hat{\psi}\nabla\hat{G}-\hat{G}\nabla\hat{\psi})\cdot\hat{n}dS=\iiint_{E}\nabla\cdot(\hat{\psi}\nabla\hat{G}-\hat{G}\nabla\hat{\psi})dV, \quad (3)$$

where $\hat{n}$ is the versor normal to the surface ∂E pointing into the outward direction of the volume E.

Reciprocity Theorem

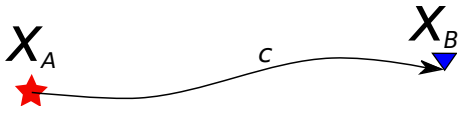

Figure 1: Sketch of a source at position x_A with a receiver at position x_B, where c is the representation of a wave path from x_A to x_B.

We consider the situation in Figure 1. Upon the use of equation (3), we deduce the reciprocity theorem for points x_A and x_B a variable-density medium.

We start from equations (1) and (2). For simplicity, we write $\hat{\psi} = \hat{\psi}(x,\omega)$ and $\hat{G}_A = \hat{G}(x,\omega;x_A)$. Multiplying equation (1) by $\hat{G}_A$, we obtain

$$\rho(x)\hat{G}_A\nabla\cdot\left[\frac{1}{\rho(x)}\nabla\hat{\psi}\right]+\frac{\omega^2}{v^2(x)}\hat{G}_A\hat{\psi}=-\hat{F}(x,\omega)\hat{G}_A, \tag{4}$$

and multiplication of equation (2) by $\hat{\psi}$ yields

$$\rho(x)\hat{\psi}\nabla\cdot\left[\frac{1}{\rho(x)}\nabla\hat{G}_A\right]+\frac{\omega^2}{v^2(x)}\hat{\psi}\hat{G}_A=-\delta(x-x_A)\hat{\psi}. \tag{5}$$

Subtracting equations (4) and (5), integrating over an arbitrary volume E, and applying Green's theorem (3), we find

$$\oiint_{\partial E}\frac{1}{\rho(x)}\left(\hat{\psi}\nabla\hat{G}_A-\hat{G}_A\nabla\hat{\psi}\right)\cdot\hat{n}dS= \iiint_E\frac{1}{\rho(x)}\left[\hat{F}(x,\omega)\hat{G}_A-\delta(x-x_A)\hat{\psi}\right]dV. \tag{6}$$

Using the Sommerfeld radiation condition, is possible demonstrate that the left-hand-side integral of the above equation tends to zero when the radius of the closed surface tends to infinity, i.e.,

$$\lim_{r\to\infty}\oiint_{\partial E(r)}\frac{1}{\rho(x)}\left(\hat{\psi}\nabla\hat{G}_A-\hat{G}_A\nabla\hat{\psi}\right)\cdot\hat{n}dS=0. \tag{7}$$

This results in the following equation for the solution to equation (1) at a point x_A,

$$\hat{\psi}(x_A,\omega)=\rho(x_A)\iiint_{\mathbb{R}^3}\frac{1}{\rho(x)}\hat{F}(x,\omega)\hat{G}_A dV. \tag{8}$$

Considering $\hat{F}(x,\omega)=\delta(x-x_B)$, we have

$$\hat{G}(x_A,\omega;x_B)=\rho(x_A)\iiint_{\mathbb{R}^3}\frac{1}{\rho(x)}\delta(x-x_B)\hat{G}(x,\omega;x_A)dV, \tag{9}$$

which results in the identity

$$\frac{\hat{G}(x_A,\omega;x_B)}{\rho(x_A)}=\frac{\hat{G}(x_B,\omega;x_A)}{\rho(x_B)}. \tag{10}$$

From the equation (10), we see that the Green function between points x_A and x_B is not reciprocal, if the values of the densities at these points are different. However, a density-scaled Green's function (Bleistein et al., 2001) is reciprocal as can be seen by multiplying each side of equation by a density factor:

$$\left[\frac{\hat{G}(x_A,\omega;x_B)}{\rho(x_A)}=\frac{\hat{G}(x_B,\omega;x_A)}{\rho(x_B)}\right]\sqrt{\rho(x_A)\rho(x_B)} \tag{11}$$

or

$$\sqrt{\frac{\rho(x_B)}{\rho(x_A)}}\hat{G}(x_A,\omega;x_B)=\sqrt{\frac{\rho(x_A)}{\rho(x_B)}}\hat{G}(x_B,\omega;x_A). \tag{12}$$

The density-scaled Green's function can then be defined as

$$\hat{g}(x,\omega;x_s)=\sqrt{\frac{\rho(x_s)}{\rho(x)}}\hat{G}(x,\omega;x_s), \tag{13}$$

where x_s is the source position. Conversely, the Green's function can be recovered from its density-scaled version by

$$\hat{G}(x,\omega;x_s)=\sqrt{\frac{\rho(x)}{\rho(x_s)}}\hat{g}(x,\omega;x_s). \tag{14}$$

Note that in the case of constant density the density-scaled Green's function $\hat{g}(x,\omega;x_s)$ reduces to the Green's function $\hat{G}(x,\omega;x_s)$ itself.

With definition (13), the reciprocity relation (12) reads

$$\hat{g}(x_A,\omega;x_B)=\hat{g}(x_B,\omega;x_A). \tag{15}$$

Interferometry

Let us now review the basic interferometry equation (see, e.g., Wapenaar et al., 2010). We consider the case where we have a closed surface with receivers located on it. Inside the enclosed volume, we have two sources located in positions x_A and x_B (see Figure 2).

We start from the complex conjugate of the Helmholtz equation (1) with a point source at x_B. With the simplified notation $G_B^* = \hat{G}^*(x,\omega;x_B)$, where the asterisk denotes the

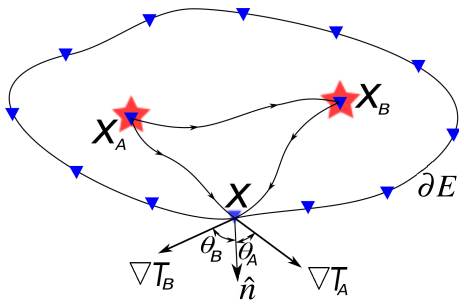

Figure 2: Sketch of two sources at positions x_A and x_B inside a volume E with receivers along the closed surface ∂E of E. Indicated at position x are the propagation directions of the incoming waves from x_A and x_B, and their angles θ_A and θ_B with respect to the unit normal vector $\hat{n}$ to the surface.

complex conjugate, the corresponding Helmholtz equation reads

$$\rho(x)\nabla\cdot\left[\frac{1}{\rho(x)}\nabla\hat{G}_B^*\right]+\frac{\omega^2}{v^2(x)}\hat{G}_B^*=-\delta(x-x_B). \quad (16)$$

Multiplying equations (2) and (16) by $\hat{G}_B^*$ and $\hat{G}_A$, respectively, and subtracting the results, we find

$$\nabla\cdot\left[\frac{1}{\rho(x)}\left(\hat{G}_A\nabla\hat{G}_B^*-\hat{G}_B^*\nabla\hat{G}_A\right)\right]=\frac{1}{\rho(x)}\left(\delta_A\hat{G}_B^*-\delta_B\hat{G}_A\right). \quad (17)$$

Integration over an arbitrary volume E, Application of Green's theorem, and consideration of the reciprocity relation (10) leads to

$$\oiint_{\partial E}\frac{1}{\rho(x)}\left(\hat{G}_A\nabla\hat{G}_B^*-\hat{G}_B^*\nabla\hat{G}_A\right)\cdot\hat{n}dS=\frac{-2i}{\rho(x_B)}Im\left[\hat{G}(x_B,\omega;x_A)\right]. \quad (18)$$

This is the fundamental relationship for all interferometry techniques, because it proves that the Green's function of the propagation from x_A to x_B can be obtained with information about the wavefield propagating from x_A and from x_B to (all) receivers on the closed surface. This only is possible if x_A and x_B are inside the closed surface.

Green's function approximation

For practical purposes, equation (18) is still inadequate, because it is extremely rare that data on closed surfaces are available. Moreover, the Green's functions' gradients generally are unknown. Therefore, the quantities in equation (18) need to be approximated by practically available data. For the following considerations, we refer again to Figure 2.

In the high-frequency situation, we can replace the Green's functions by their asymptotic $WKBJ$ approximation,

$$\hat{G}(x,\omega;x_s)\approx L(x;x_s)\exp\left[-i\omega T(x;x_s)\right]. \quad (19)$$

There, T is the traveltime from x_s to x which satisfies the eikonal equation $\|\nabla T(x;x_s)\|^2=\frac{1}{v^2(x)}$ and $L(x;x_s)$ is the geometrical spreading. Still in high-frequency approximation the Green's function's gradient can be approximated by

$$\nabla\hat{G}(x,\omega;x_s)\approx-i\omega\hat{G}(x,\omega;x_s)\nabla T. \quad (20)$$

Substituting equations (19) and (20) in (18) and defining $\Theta(x;x_A,x_B)=\frac{\cos\theta_A+\cos\theta_B}{2v(x)}$, we obtain

$$-\omega\rho(x_B)\oiint_{\partial E}\frac{1}{\rho(x)}\hat{G}_A\hat{G}_B^*\Theta(x;x_A,x_B)dS\approx Im\left[\hat{G}(x_B,\omega;x_A)\right]. \quad (21)$$

Assuming that the surface is sufficiently far from the points x_A e x_B, we can approximate $\theta\approx\frac{1}{v(x)}$. Thus, in far-field approximation, we can write

$$-\omega\rho(x_B)\oiint_{\partial E}\frac{1}{\rho(x)v(x)}\hat{G}_A\hat{G}_B^*dS\approx Im\left[\hat{G}(x_B,\omega;x_A)\right]. \quad (22)$$

Considering the equations (13) and (15), we can recast equation (22) into the form

$$-\omega\oiint_{\partial E}\frac{1}{v(x)}\hat{g}(x_A,\omega;x)\hat{g}^*(x_B,\omega;x)dS\approx Im\left[\hat{g}(x_A,\omega;x_B)\right]. \quad (23)$$

Equation (23) shows that the situation of Figure 2 can be exchanged for one where instead of sources inside the volume, there are receivers, and instead of receivers at the surface, there are sources. This is the reciprocity principle (see Figure 3).

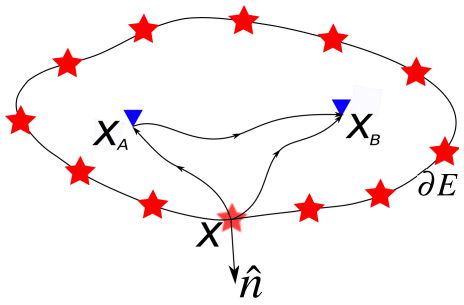

Figure 3: Sketch of two receivers inside a volume E at positions x_A and x_B and sources along the closed surface ∂E of E.

Redatuming

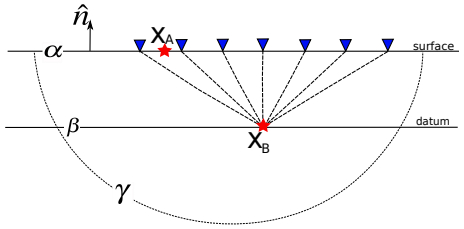

Figure 4: Sketch of the surface parts α and γ. Also shown is datum β as a reference to the redatuming of the array at the surface.

Considering the theoretical part above, we can imagine that the surface ∂E in the Figure 2 can be divided into two surfaces α and γ (see Figure 4). The surface α contain the sources and receivers of a conventional seismic array, and γ is a surface part that is needed to close it. Also shown in Figure 2 is a reference surface β for redatuming, where a new source is located.

We suppose that seismic data have been aquired for sources at points x_A and receivers along the seismic array, and that a velocity model is known for the medium between surfaces α and β so that the direct wave from all points x_B on β to all points on α can be estimated by seismic modeling. We will show in this section that cross-correlation of this modeled direct waves with the seismic surface data allows to approximately redatum the acquisition array (sources and receivers) to reference datum β.

The total Green's function for the wavefield at surface α can be decomposed in a unique way as $\hat{G}=\hat{G}^i+\hat{G}^s$ (Bleistein et al., 2001), where $\hat{G}^i$ is the solution of the wave equation in some reference medium and $\hat{G}^s$ is the difference to the

complete solution in the medium under consideration. For a point source at x_A, $\hat{G}^i_A = \hat{G}^i(x,\omega;x_A)$ must satisfy

$$\mathscr{L}_0 \hat{G}^i_A = -\delta(x - x_A), \tag{24}$$

where $\mathscr{L}_0$ is the Helmholtz operator for the reference medium, involving the density ρ_0 and and velocity v_0 instead of ρ and v.

The scattering field $\hat{G}^s_A = \hat{G}^s(x,\omega;x_A)$ must then satisfy a perturbed wave equation that can be written as

$$\mathscr{L}_0 \hat{G}^s_A = -\mathscr{V}(x)\left[\hat{G}^i_A + \hat{G}^s_A\right], \tag{25}$$

where $\mathscr{V}(x) = \mathscr{L} - \mathscr{L}_0$ is the difference between the perturbed and uperturbed Helmholtz operators, called the perturbation operator or scattering potential (Rodberg and Thaler, 1967).

Using equations (24) and (25), we can set up an equation similar to equation (17). For this purpose, we multiply equation (25) with G^{i*}_B and the complex conjugate of equation (24) for a point source at x_B with G^s_A. Subtracting the results, we arrive at

$$\nabla\cdot\left[\frac{1}{\rho_0(x)}\left(\hat{G}^s_A\nabla\hat{G}^{i*}_B - \hat{G}^{i*}_B\nabla\hat{G}^s_A\right)\right] = \frac{1}{\rho_0(x)}\left(\hat{G}^{i*}_B\mathscr{V}\hat{G}_A - \delta_B\hat{G}^s_A\right). \tag{26}$$

After application of Green's theorem, this yields

$$\oiint_{\alpha+\gamma}\frac{1}{\rho_0(x)}\left(\hat{G}^s_A\nabla\hat{G}^{i*}_B - \hat{G}^{i*}_B\nabla\hat{G}^s_A\right)\cdot\hat{n}dS = \iiint_E \frac{\hat{G}^{i*}_B\mathscr{V}\hat{G}_A}{\rho_0(x)}dV - \frac{\hat{G}^s_{BA}}{\rho_0(x_B)}. \tag{27}$$

Taking the surface γ in equation (27) to represent the lower semisphere with radius r, we can write

$$\iint_\gamma \frac{1}{\rho_0(x)}\left(\hat{G}^s_A\nabla\hat{G}^{i*}_B - \hat{G}^{i*}_B\nabla\hat{G}^s_A\right)\cdot\hat{n}dS \approx \int_0^{2\pi}\int_0^{\pi/2}\frac{r\hat{G}^s_A}{\rho_0(x)}r\left(\frac{i\omega}{v_0(x)}\cos\theta_A\hat{G}^{i*}_B + \frac{\partial\hat{G}^{i*}_B}{\partial r}\right)d\Omega. \tag{28}$$

where $d\Omega = \sin\theta d\theta d\phi$ is the differential of the solid angle. According to Wapenaar's radiation condition, this integral can be considered as tending to zero when r tends to infinity.

Therefore, only integration along surface α remains in equation (27). After high-frequeny approximations analogous to equations (19) and (20), equation (27) allows to approximately calculate the scattered field at x_B as

$$\hat{g}^s(x_B,\omega;x_A) \approx i\omega\iint_\alpha \frac{\hat{g}^s_A\hat{g}^{i*}_B}{v_0(x)}dS + \hat{I}_{BA}, \tag{29}$$

where

$$\hat{I}_{BA} = \iiint_E \hat{g}^{i*}_B\mathscr{V}\hat{g}_A dV\ , \tag{30}$$

denotes an undesired scattering term that gives rise to spurious events.

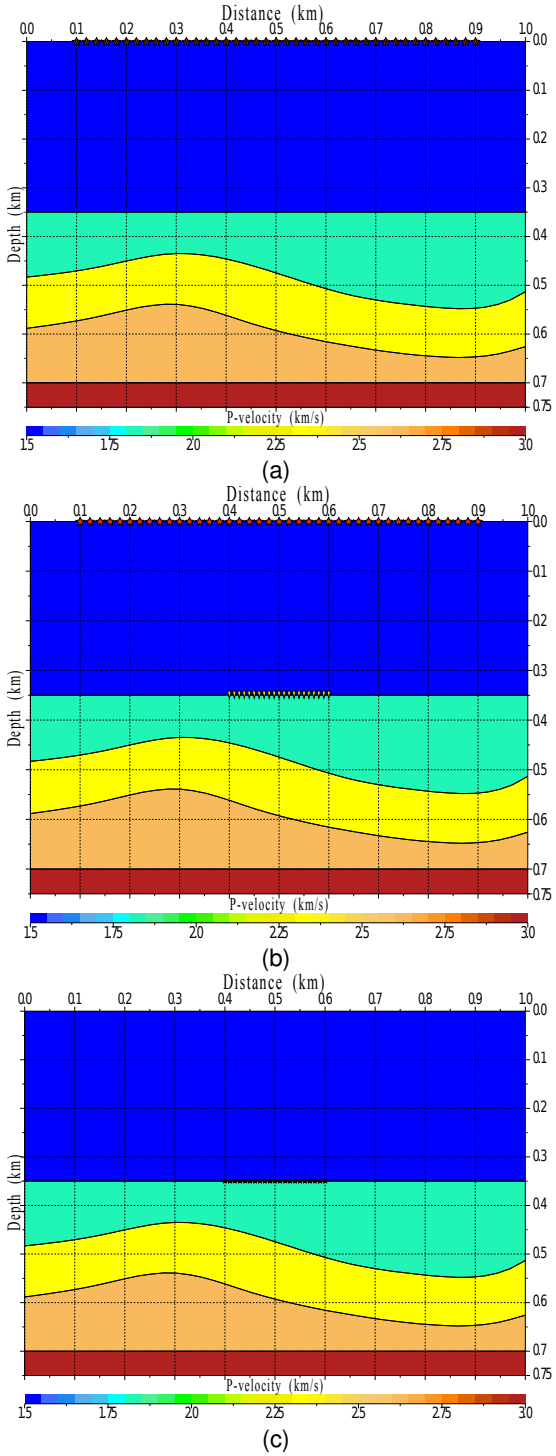

Figure 5: Modeling seismic data considering: (a) array of sources and receivers on the surface, (b) array of the sources on the surface and receivers at 350m of depth and (c) all array redatuming at 350m of depth.

Equation (29) is the principal theoretical result of this work. It states that it is possible to redatum surface data by means of interferometry using direct-wave modeling. This equation allows to obtain the Green's function at x_B for a point source at x_A by the cross-correlation of the modeled direct wave in x_B with the acquired wavefield in x_A.

Numerical modeling

To numerically validate the interferometry-redatuming equation (29) derived in this work, we devised three experiments, synthetically simulating a marine-seismic situation. The 2D model is 1 km long and 750 m deep (see Figure 5 and consists of a flat ocean bottom at 350 m depth and two curved and a planar reflector below. The velocities range from 1500 m/s in the water to 3000 m/s in the lowermost layer. The seismic experiments consider three situations: (1) shots and receivers at the surface (Figure 5a), (2) shots at the surface and receivers at the ocean bottom (Figure 5b) and (3) shots and receiver at the ocean bottom (Figure 5c). The synthetic seismic data and the direct waves needed for the redatuming process were modeled using Norsar's ray-tracing code.

The seismic array on the surface consisted of sources and receivers spaced at 20 m, covering the range between 100 m and 900 m (Figure 5a). The source array for the second experiment is the same, and the receiver array at 350 m depth covers the space between 400 m and 600 m, spaced at 10 m (Figure 5b). The final experiment used both sources and receivers at these positions at 350 m depth (Figure 5c). The wavelet used for the synthetic seismograms was a Ricker wavelet of 50 Hz. For simplicity, we considered constant density in all layers.

Results

Figure 6 compares the results of interferometry redatuming the data from experiment 1 to the configuration of experiment 2 using equation (29) (Figure 6b) to the modeled data (Figure 6a). For this purpose, we modeled the direct waves from all receivers at depth to all source positions at the surface. Shown in Figure 6 are all common-receiver gathers at the new depth. We see that the kinematic properties of the data are nicely matched, while the amplitudes have suffered some alterations.

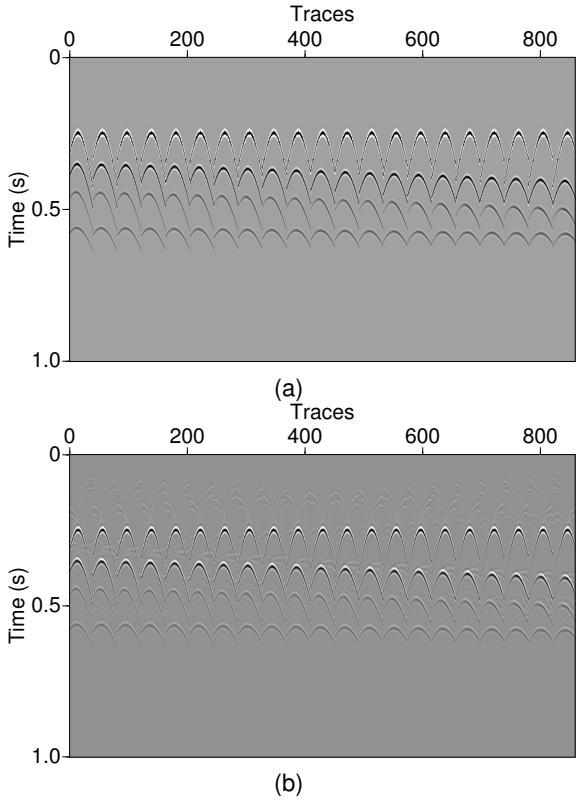

Figure 6: Seismic interferometry redatuming of data from the numerical model of Figure 5. (a) Modeled seismic data at depth; (b) redatumed data, i.e., seismic surface data cross-correlated with the modeled direct wave.

For a more detailed analysis of the dynamic properties, Figure 7 compares the redatumed trace at the center of both the source and receiver arrays to the modeled one. We see that the principal difference in amplitudes is the direct wave, which is not covered by the theoretical development. The amplitudes of the reflected events are comparable.

The data of Figure 6 have then been used as an input to a second redatuming step to to acquisition geometry completely at the ocean bottom. Figure 8 compares the resulting zero-offset sections to the modeled data at depth. We see that the one-step redatuming of the ocean-bottom-receiver data (Figure 8b) recovers the modeled data (Figure 8a) quite nicely. Though the two-step redatuming of the surface data introduces some noise and weak spurious events, the three reflection events are still correctly positioned.

The trace-to-trace comparison at midpoint coordinate 500 m (Figure 9) reveals that positions and relative amplitudes of the three reflection events are correctly recovered by both the one-step and two-step redatuming procedures. The interferometric wavelet changes by the correlations, and some noise becomes visible in the two-step result (Figure 9c).

Conclusions

In this work, we have developed an interferometric redatuming technique that uses the correlation of direct waves in a reference model with scattered waves in the true model to reposition sources and/or receivers for the latter. For this purpose, we started at the Helmholtz equation with density variation and reformulated the reciprocity theorem for this situation.

We have tested the resulting redatuming technique on synthetic seismic data from a three-layer model. We simulated surface-seismic data, ocean-bottom-receiver data, and a complete ocean-bottom acquisition for

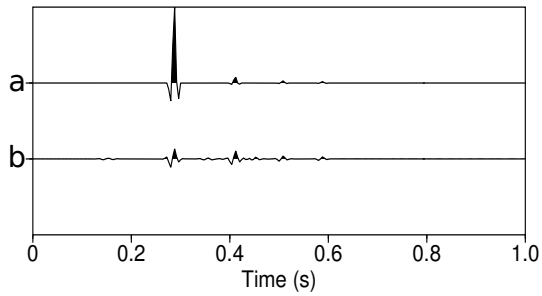

Figure 7: Comparison of trace 400 from Figures 6a and b. (a) Modeled trace with sources at the surface and receivers at 350 m depth; (b) interferometric redatuming trace, obtained from correlating the direct wave with the data acquired at the surface.

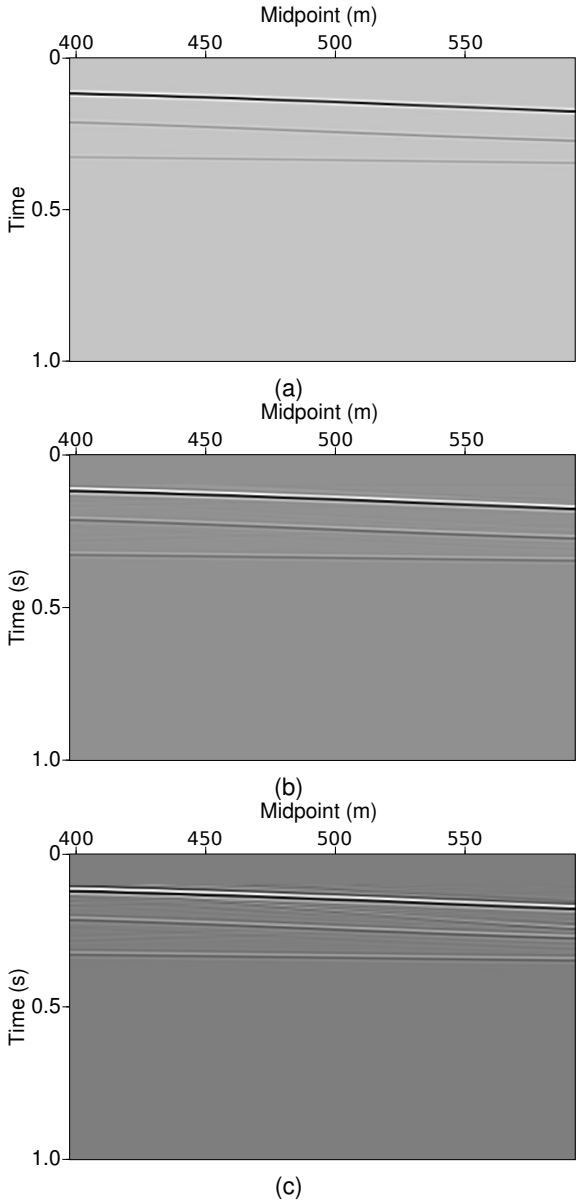

Figure 8: Zero-offset sections at the ocean bottom. (a) Seismic data modeled with sources and receivers at depth, (b) one-step interferometric redatuming of data with sources at the surface and receivers at depth; (c) two-step interferometric redatuming of data with sources and receivers at the surface. Direct waves have been muted for display.

comparison. In a first step, we redatumed the receivers of the surface data to the ocean bottom and compared the results to the data modeled with this geometry. We found that the reflected events were correctly recovered in position and amplitude. In a second step, we redatumed the sources of both the modeled and redatumed ocean-bottom-receiver data. While in this step, again all reflection events were treated correctly, we found that the two-step redatuming of the surface data introduced some noise and spurious events.

The correlation with the direct wave only has the advantage that this wave is generally easily accessible. If ocean-bottom or borehole receivers are available, the direct wave can be measured, or if a reference velocity model down

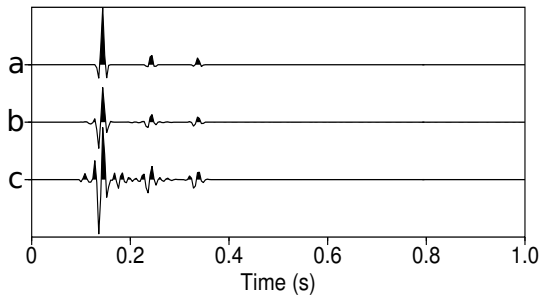

Figure 9: Comparison of trace at midpoint coordinate 500 m of Figure 8. (a) Data modeled at depth; (b) Source interferometric redatuming of data with source at the surface and receivers at depth; (c) two-step interferometric redatuming of surface data.

to a desirable datum is known, it can be determined by modeling.

Acknowledgments

This work was kindly supported by the Brazilian research agencies CAPES and CNPq as well as Petrobras and the sponsors of the Wave Inversion Technology (WIT) Consortium.

References

Bleistein, N., J. K. Cohen, and J. W. S. Jr., 2001, Mathematics of Multidimensional Seismic Imaging, Migration, and Inversion: Springer.

Claerbout, J., 1968, Synthesis of a layered medium from its acoustic transmission response: Geophysics, **33**, 264–269.

Dong, S., X. Xiao, Y. Luo, and G. Schuster, 2007, 3D target-oriented reverse time datuming: SEG Expanded Abstracts, **26**, 2442–2445.

Green, G., 1828, An eassy on the application of mathematical analysis to the theories of electricity and magnetism: Privately published.

Lu, R., M. Willis, X. Chapman, J. Ajo-Franklin, and M. N. Toksöz, 2008, Redatuming through a salt canopy and target-oriented salt-flank imaging: Geophysics, **73**, S63–S71.

Rodberg, L. S., and R. M. Thaler, 1967, Introduction to the quantum theory of scattering: Academic Press.

Scherbaum, F., 1978, Seismic imaging of the site response using microearthquake recordings. Part II. Aplication to the Swabian Jura, southwest Germany, seismic network: Bulletin of Seismological Society of America, **77**, 1924–1944.

Schuster, G., and M. Zhou, 2006, A theoretical overview of model- based and correlation-based redatuming methods: Geophysics, **71**, SI103–SI110.

van der Neut, J., J. Thorbecke, K. Mehta, E. Slob, and K. Wapenaar, 2011, Controlled-source interferometric redatuming by crosscorrelation and multidimensional deconvolution in elastic media: Geophysics, **76**, SA63–SA76.

Wapenaar, K., D. Draganov, R. Snieder, X. Campman, and A. Verdel, 2010, Tutorial on seismic interferometry: Part 1 - basic principles and applications: Geophysics, **75**, 75A195–75A209.

Xiao, X., and G. Schuster, 2006, Redatuming CDP data below salt with VSP Green's function: SEG Expanded Abstracts, **25**, 3511–3515.